nature materials

LETTERS

PUBLISHED ONLINE: 12 AUGUST 2012 | DOI: 10.1038/NMAT3401

Quantum effect on thermally activated glide of dislocations

Laurent Proville[1], David Rodney[2]* and Mihai-Cosmin Marinica[1]

Crystal plasticity involves the motion of dislocations under stress. So far, atomistic simulations of this process have predicted Peierls stresses[1], the stress needed to overcome the crystal resistance in the absence of thermal fluctuations, of more than twice the experimental values, a discrepancy best-known in body-centred cubic crystals[2–4]. Here we show that a large contribution arises from the crystal zero-point vibrations, which ease dislocation motion below typically half the Debye temperature. Using Wigner's quantum transition state theory[5,6] in atomistic models of crystals, we found a large decrease of the kink-pair formation enthalpy due to the quantization of the crystal vibrational modes. Consequently, the flow stress predicted by Orowan's law[7] is strongly reduced when compared with its classical approximation and in much closer agreement with experiments. This work advocates that quantum mechanics should be accounted for in simulations of materials and not only at very low temperatures or in light-atom systems.

Crystals, simply because they are made of atoms, impose a resistance to the motion of their dislocations. This resistance is characterized by the so-called Peierls stress[1], measured experimentally as the zero-temperature limit of the flow stress of well-annealed crystals[8,9]. Depending on the dislocation core structure, the Peierls stress may be negligibly small, as for $a/2\langle 110\rangle\{111\}$ dislocations in face-centred cubic (fcc) crystals, but it may also be appreciably large, as for $a/2\langle 111\rangle$ screw dislocations in body-centred cubic (bcc) crystals. In the latter case, dislocation glide proceeds at low temperature through the Peierls mechanism, where thermal fluctuations in the crystal vibrations occasionally induce the nucleation of a pair of kinks on straight dislocations (Fig. 1). The kinks then glide at high velocity along the dislocation line, allowing the whole dislocation to advance to the next equilibrium position, called a Peierls valley.

Atomistic calculations of the Peierls stress have so far been based on classical mechanics. However, already in 1971, from early simulations of bcc sodium, it was reported that the Peierls stress of screw dislocations was 0.01μ (μ is the elastic shear modulus), much larger than experimental data, between 0.002 and 0.0033μ. Since then, similar discrepancies have been reported in a wide range of bcc crystals[3,10,11], notwithstanding the use of electronic structure methods to accurately represent atomic bonding[12,13] or boundary conditions adapted to dislocations[12,14]. In the case of bcc iron modelled in Fig. 1, the computed Peierls stress is 0.9 GPa (Fig. 2), compared with 0.4 GPa obtained experimentally[8,9]. Several theories have been proposed to explain this discrepancy, invoking collective dislocation dynamics[15] and dislocation junctions[16]. These processes are unquestionably at play during plastic flow, but they only partially solve the discrepancy because they are, for example, absent from recent low-temperature *in situ* observations[17], where the stress level remains small compared with atomistic simulations.

To reduce the thermal activation, the experiments to measure the Peierls stress are performed at low temperatures where quantum effects are possible. Dislocation zero-point vibration[3,4,18] and tunnelling[18,19] have been considered theoretically in phenomenological models where the dislocation is viewed as a single particle or an elastic string. These models, however, rely on a very simplified description of some essential features, particularly the atomistic structure of the dislocation core and the quantum dynamics of the crystal itself, and cannot provide a quantitative explanation for the discrepancy between simulated and experimental Peierls stresses. Here we apply a fully atomistic approach to analyse how quantum statistics contribute to the thermally activated glide of dislocations.

To address a specific case, we consider first an atomic model of bcc iron based on a recent many-body embedded atom method (EAM) interatomic potential[20], which provides a satisfactory description of the dislocation core geometry and glide process in comparison with electronic-structure first-principles calculations[21]. The latter method cannot be employed here because of the large number of atoms ($N = 123{,}120$) required to model kink pairs without strong finite-size effects. The case of bcc iron can be considered as prototypical of other bcc crystals where first-principles calculations show similar dislocation features[12,13]. Two examples of classical computation of the minimum enthalpy path for the nucleation and propagation of a kink pair on a screw dislocation are reported in Fig. 2a at different applied shear stresses τ_{yz}. The calculations are based on the nudged elastic band method (see ref. 22 and Methods section for details). The maximum along the paths is the activated state, consisting of a dislocation with a critical kink pair. The corresponding enthalpy, the kink-pair formation enthalpy H_{kp}, is plotted in Fig. 2b against τ_{yz}. As can be seen, the formation enthalpy falls down to zero at a stress limit of 0.9 GPa, which defines the classical Peierls stress for the present energy model.

The rate of barrier crossing, $\Gamma_{\mathrm{classic}}$, which controls the dislocation velocity $v = a\Gamma_{\mathrm{classic}}$ (a is the distance between Peierls valleys) can be expressed in classical mechanics using the harmonic transition state theory[23] (TST):

$$\Gamma_{\mathrm{classic}} = L\sqrt{\frac{2\pi m}{kT}}\frac{\prod_{i=1}^{3N-3}\nu_i^{\mathrm{init}}}{\prod_{k=2}^{3N-4}\nu_k^{*}}\exp\left(-\frac{H_{\mathrm{kp}}(\tau_{yz})}{kT}\right) \qquad (1)$$

The first term of the pre-exponential factor in equation (1), $L\sqrt{2\pi m/kT}$, arises from the Goldstone mode because the stresses applied here are above the secondary Peierls stress, resulting in free kink motion along the dislocation line (L is the dislocation length and m is the atomic mass). The second term, $\prod_{i=1}^{3N-3}\nu_i^{\mathrm{init}}/\prod_{k=2}^{3N-4}\nu_k^{*}$,

[1]CEA, DEN, Service de Recherches de Métallurgie Physique, Gif-sur-Yvette 91191, France, [2]Laboratoire de Science et Ingénierie des Matériaux et Procédés, Grenoble Institute of Technology, CNRS, UJF, Saint Martin d'Hères 38402, France. *e-mail: David.Rodney@grenoble-inp.fr.

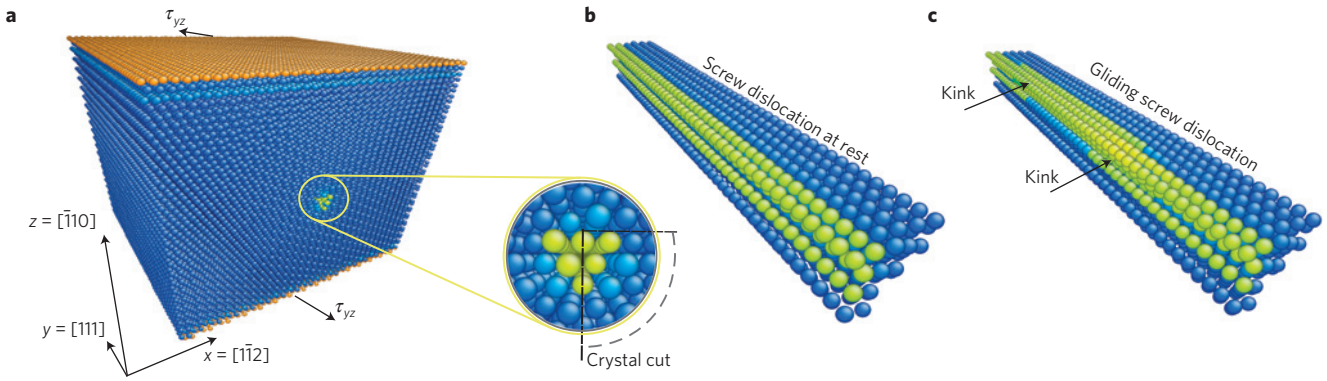

Figure 1 | Peierls mechanism of dislocation glide. A bcc iron crystal containing a screw dislocation is modelled with the interatomic potential proposed in ref. 20. **a**, Simulation cell. Atoms are coloured according to their potential energy and a τ_{yz} shear stress is applied to the free surfaces[14] (orange atoms). A crystal cut-through allows visualization of the atoms near the dislocation core (green–yellow atoms). **b**, Straight dislocation at rest. **c**, The dislocation glides through the nucleation and subsequent expansion of a kink pair.

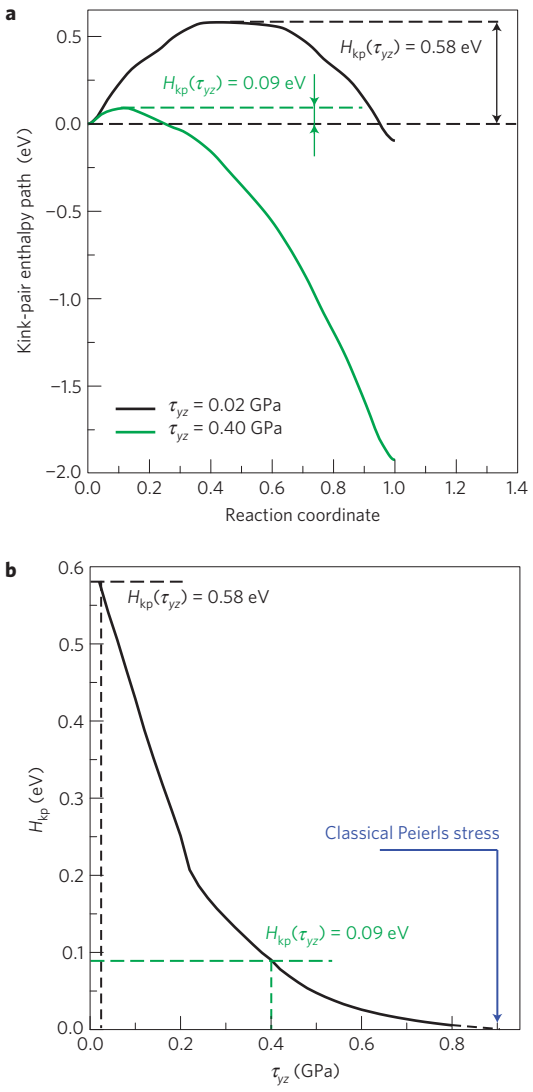

Figure 2 | Kink-pair enthalpy. a, Classical kink-pair minimum enthalpy path of a screw dislocation in iron, obtained at two different applied stresses using the nudged elastic band method[22]. **b**, Variation of the kink-pair formation enthalpy, the maximum enthalpy along the minimum enthalpy path, as a function of applied stress.

is the ratio of the partition functions of the harmonic vibrational modes of the crystal with real non-zero frequencies, $\{\nu_k^*\}$ and $\{\nu_i^{\text{init}}\}$, computed in the activated and initial states respectively, by diagonalizing the Hessian matrix of the system (see Methods).

It was shown[5] that quantum effects can be estimated within a harmonic TST by treating the vibrational modes quantum mechanically. Zero-point vibrations are included by replacing the classical oscillator partition functions by their quantum analogues and thermally assisted tunnelling near the top of the energy barrier is introduced by means of the transmission factor through the parabolic barrier associated with the unstable mode of the saddle configuration, of imaginary frequency $i\nu_{\text{US}}^*$. The resulting expression is (see ref. 24 and Supplementary Information for details):

$$\Gamma_{\text{quantum}} = L\sqrt{\frac{2\pi m}{kT}}\frac{h\nu_{\text{US}}^*/2kT}{\sin\left(h\nu_{\text{US}}^*/2kT\right)}\left(\frac{kT}{h}\right)^2 \times \frac{\prod_{i=1}^{3N-3}2\sinh\left(h\nu_i^{\text{init}}/2kT\right)}{\prod_{k=2}^{3N-4}2\sinh\left(h\nu_k^*/2kT\right)}\exp\left(-\frac{H_{\text{kp}}\left(\tau_{yz}\right)}{kT}\right) \quad (2)$$

The second term in the above expression, the transmission factor, diverges at a crossover temperature $T_{\text{tun}} = h\nu_{\text{US}}^*/2\pi k$, below which is the athermal deep tunnelling regime where the above approximation breaks down[24]. In the present calculations, T_{tun} lies between 1 and 6 K depending on the applied stress, thus limiting deep tunnelling to very low temperatures. Above T_{tun}, the transmission factor is close to unity and may be discarded in equation (2). In this regime, the quantum rate can be rewritten as a correction, δE, to the classical rate, known as Wigner correction[6]:

$$\Gamma_{\text{quantum}} = \exp\left(\frac{\delta E}{kT}\right)\Gamma_{\text{classic}} \quad \text{with}$$
$$\delta E = kT\ln\left(\frac{\prod_{i=1}^{3N-3}2\sinh\left(h\nu_i^{\text{init}}/2kT\right)/\left(h\nu_i^{\text{init}}/kT\right)}{\prod_{k=2}^{3N-4}2\sinh\left(h\nu_k^*/2kT\right)/\left(h\nu_k^*/kT\right)}\right) \quad (3)$$

As illustrated in Fig. 3a, Wigner correction deviates from zero over a wide temperature range. The transition temperature between quantum and classical regimes is half the Debye temperature, above which all hyperbolic sine functions in equation (3) can be replaced by their arguments. In this high-temperature regime where most experiments are performed, the present calculations are thus fully consistent with the classical TST of equation (1). In the low-

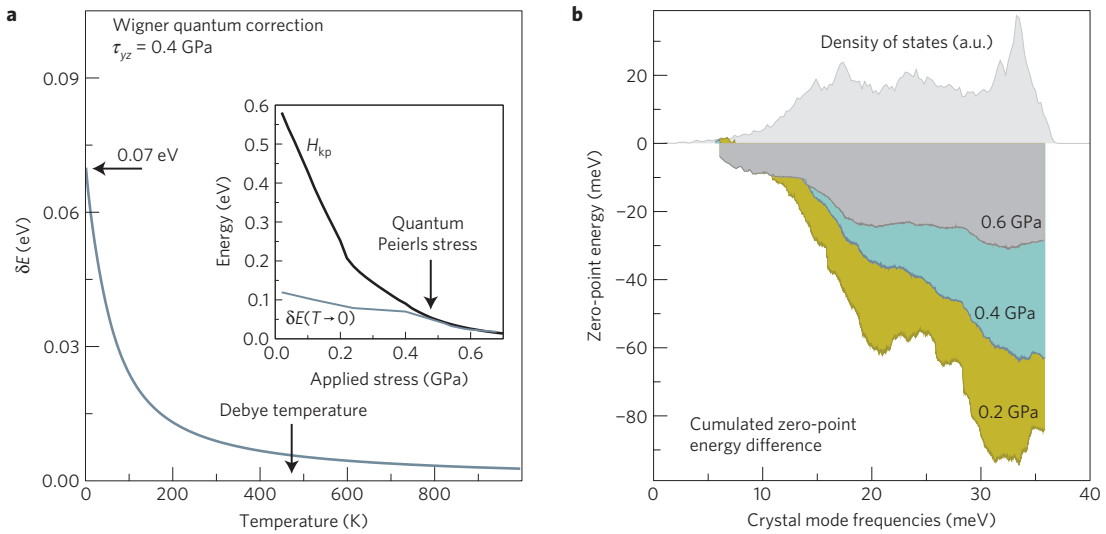

Figure 3 | Quantum effects on kink-pair formation. a, Temperature variation for the quantum correction δE at an applied stress of 0.4 GPa. In the inset, variation of the kink-pair formation enthalpy and correction term in the zero-temperature limit as a function of applied stress. **b**, Cumulated zero-point energy difference between the vibrational modes of the crystal with a dislocation containing a kink pair in the transition state and the crystal with a straight dislocation in equilibrium, against mode frequency. The phonon density of states with the same iron model is also reported.

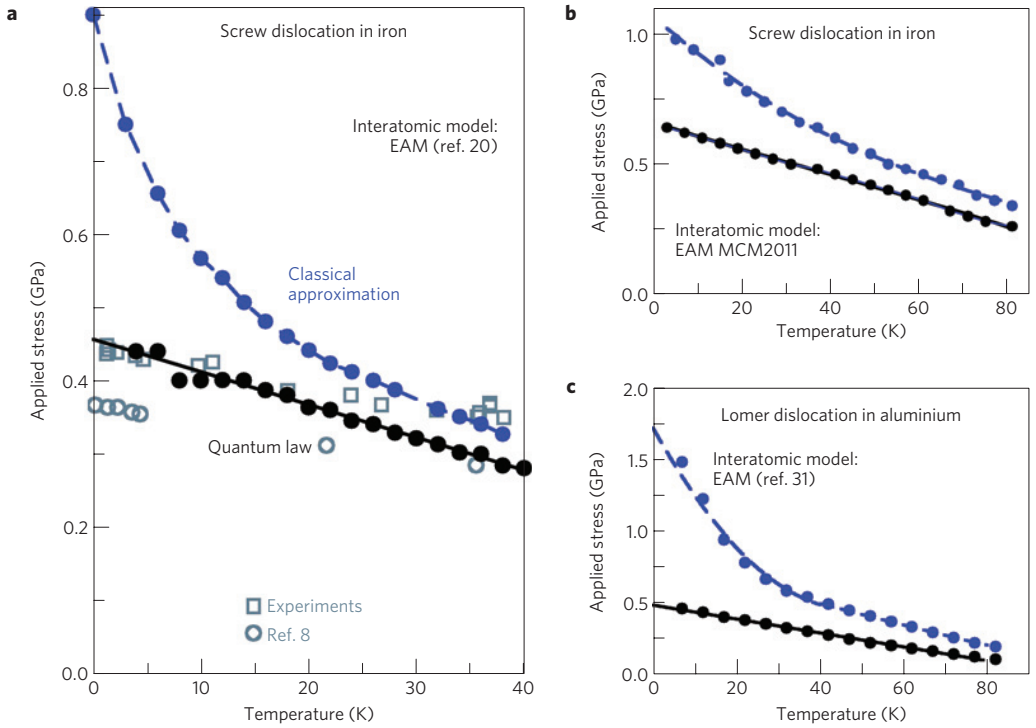

Figure 4 | Quantum Orowan law. a, Comparison of the temperature dependence of the applied stress predicted by the quantum Orowan law (solid curve), its classical approximation (dashed curve) and experimental data obtained with two crystal orientations in iron (open symbols)[8]. **b**, The same computations as in **a** with a different energetic model of iron, MCM2011 (see Supplementary Information). **c**, The same computations as in **a** for a different system, an $a/2\langle 110\rangle\{001\}$ edge Lomer dislocation in fcc aluminium[14].

temperature limit, the correction converges to the commonly used zero-point energy correction[6,25] $\sum_{i=1}^{3N-3} h\nu_i^{\text{init}}/2 - \sum_{k=2}^{3N-4} h\nu_k^*/2$. As shown in the inset of Fig. 3a, this limit increases with decreasing stress and is of the order of 0.1 eV, a significant fraction of the enthalpy H_{kp}. Corrections of the same order have been obtained for other processes, for instance surface adsorption[6] and diffusion[25]. As a result and as shown in the inset of Fig. 3a, the effective enthalpy $H–\delta E$ becomes zero with the present iron model at an applied stress, which defines the quantum Peierls stress, close to 0.4 GPa. This stress is roughly half the classical Peierls stress, 0.9 GPa (Fig. 2b), in good agreement with the experimental value. To identify the physical origin of the quantum correction, we analysed the contribution of the different vibrational modes to the zero-point energy difference. We found that the main contribution comes from modes localized near the dislocation core. Typically, 90% of the correction is recovered when considering partial Hessian matrices restricted to the atoms within 0.7 nm of the dislocation core. However,

it seems from Fig. 3b that the quantum correction cannot be attributed to specific modes among those localized modes. Instead, the total cumulated zero-point energy difference arises from small modifications of many modes perturbed by the presence of the kink pair, with frequencies spreading over the entire phonon spectrum indicated by the density of state of the full crystal reported in Fig. 3b.

To compare with experiments at finite temperature, the plastic strain rate $\dot{\varepsilon}$ may be computed from the dislocation velocity using the Orowan equation[7], $\dot{\varepsilon} = \rho b v = \rho b a \Gamma$, where ρ is the dislocation density and b is the dislocation Burgers vector. Using the experimental value[8] for the strain rate ($\dot{\varepsilon} = 8 \times 10^{-5}\,s^{-1}$) and a dislocation density of $\rho = 10^{10}\,m^{-2}$ (this parameter has little influence and can be increased to $10^{12}\,m^{-2}$ without noticeable effect), the above relation can be inverted numerically to obtain the flow stress as a function of temperature, using either the quantum rate (equation (2)) or its classical approximation (equation (1)). Results are shown in Fig. 4a. In the zero-temperature limit, the quantum law tends to the quantum Peierls stress (Fig. 3a inset) whereas the classical approximation tends to the classical Peierls stress (Fig. 2b). The deviation between the quantum and classical laws decreases gradually over a broad range of temperatures, consistent with the quantum correction shown in Fig. 3a. Figure 4a compares our results with experimental data[8]. The agreement is particularly good with the present potential. To check the dependence of the correction on the energetic model, we developed a new interatomic potential, which predicts more accurately the screw dislocation Peierls potential (see Supplementary Information). The result is shown in Fig. 4b, confirming the large quantum correction at low temperatures. The new Peierls stress is 0.2 GPa above the experimental data. Such variability is expected among semi-empirical interatomic potentials, but it should be noted that the difference remains smaller than the 0.4 GPa decrease predicted with both potentials between classical and quantum Peierls stresses. Therefore, the quantum correction may not account for the entire discrepancy between simulations and experiments, but provides at least a large contribution. Note also that for both potentials, the flow stress with quantum correction decreases linearly with increasing temperature, in agreement with experimental data and in contrast with the classical law. To confirm the generality of the quantum effect discussed here and show that it is not limited to iron nor to bcc screw dislocations, the same effect is confirmed in Fig. 4c for a Lomer dislocation in a fcc crystal of aluminium (Fig. 4c). This dislocation is a non-conventional $a/2\langle 110\rangle\{001\}$ edge dislocation whose high Peierls stress is partly responsible for the strength of Lomer–Cottrell dislocation junctions[14].

The discrepancy between experimental and simulated Peierls stresses arises mainly from the quantum statistics of the crystal vibrational modes. Further theoretical improvements should include electronic structure methods, based on the density functional theory[12,21] or for instance bond order potentials[26] to reduce uncertainties related to the interatomic potential. The present work shows the importance of accounting for quantum effects when simulating crystal plasticity at low temperature and may also provide a theoretical basis for interpreting recent *in situ* observations of a low-temperature jerky dislocation glide regime[17]. Other plasticity processes should be revisited, including dislocation glide in covalent crystals[27], solid solutions[28] and dislocation nucleation from thermally activated sources, where vibrations also play an important role[29]. Finally, the quantum correction used here applies in principle to all thermally activated processes and is expected to be significant if the energy barrier is small enough that the corresponding kinetics remains measurable experimentally at low temperatures. In this context, vacancy migration[30] is another process worth investigating in detail.

Methods

Classical kink-pair formation. The simulation cell has bcc symmetry with 20, 54 and 22.5 repeating units in directions x[211], y[111] and z[011], respectively ($N = 123,120$ atoms). Periodic boundary conditions are applied in directions x and y (with fixed cell dimensions) whereas the z surfaces are free. A screw dislocation with Burgers vector $b = a/2$[111] is introduced along the central [111] axis of the cell by means of its elastic displacement field, followed by energy minimization. A shear stress τ_{yz} is applied on the {011}[111] slip system by adding external forces to the atoms in the upper and lower z surfaces[14].

The minimum enthalpy path between successive equilibrium configurations of the dislocation in direction x is computed using the climbing nudged elastic band method[14,22] with an improved tangent calculation to minimize the total energy of a chain of 90 crystal replicas linked by harmonic springs of strength 10 eV Å^{-1}. We further asserted the validity of the transition states by checking that they were first-order saddle points (with a force of less than 10^{-2} eV nm^{-1} and a single negative eigenvalue) and checking their connectivity to the initial and final states by re-relaxations following forward and backward perturbations along the eigenvector of the imaginary mode.

Harmonic vibrational frequencies. Normal-mode frequencies in equations (1)–(3) are computed by diagonalizing the Hessian matrix of the initial equilibrium and activated states of the dislocation at each applied stress. Exact diagonalizations were performed using ScaLAPACK parallel routines on 2,304 central processing units. We checked that the correction in equation (3) does not depend appreciably on cell dimensions in the range accessible to our computational capabilities.

Received 1 May 2012; accepted 13 July 2012; published online 12 August 2012

References

1. Peierls, R. E. On the size of a dislocation. *Proc. Phys. Soc. Lond.* **52,** 34–37 (1940).
2. Basinski, Z. S., Duesbery, M. S. & Taylor, R. Influence of shear stress on screw dislocations in a model sodium lattice. *Can. J. Phys.* **49,** 2160–2180 (1971).
3. Suzuki, H. in *Fundamental Aspects of Dislocation Theory* (eds Simmons, J. A., de Wit, R. & Bullough, R.) 253–272 (Spec. Publ. 317, Nat. Bur. Stand., 1970).
4. Takeuchi, S., Hashimoto, T. & Maeda, K. Plastic deformation of bcc metal single crystals at very low temperatures. *Trans. Jpn Inst. Met.* **23,** 60–69 (1982).
5. Wigner, E. The transition state method. *Trans. Faraday Soc.* **34,** 29–41 (1938).
6. Henkelman, G., Arnaldsson, A. & Jónsson, H. Theoretical calculations of CH_4 and H_2 associative desorption from Ni(111): Could subsurface hydrogen play an important role? *J. Chem. Phys.* **124,** 044706 (2006).
7. Orowan, E. Problems of plastic gliding. *Proc. Phys. Soc.* **52,** 8–22 (1940).
8. Kuramoto, E., Aono, Y., Kitajima, K., Maeda, K. & Takeuchi, S. Thermally activated slip deformation between 0.7 and 77 K in high-purity iron single crystals. *Phil. Mag. A* **39,** 717–724 (1979).
9. Brunner, D. & Diehl, J. Extension of measurements of the tensile flow stress of high-purity α-iron single crystals to very low temperatures. *Z. Metalkd.* **83,** 828–834 (1992).
10. Marian, J., Cai, W. & Bulatov, V. V. Dynamic transitions from smooth to rough to twinning in dislocation motion. *Nature Mater.* **3,** 158–163 (2004).
11. Chaussidon, J., Fivel, M. & Rodney, D. The glide of screw dislocations in bcc Fe: Molecular statics and dynamics simulations. *Acta Mater.* **54,** 3407–3416 (2006).
12. Woodward, C. & Rao, S. I. Flexible *ab initio* boundary conditions: Simulating isolated dislocations in bcc Mo and Ta. *Phys. Rev. Lett.* **88,** 216402 (2002).
13. Li, J. *et al.* Core energy and Peierls stress of a screw dislocation in bcc molybdenum: A period-cell tight-binding study. *Phys. Rev. B* **70,** 104113 (2004).
14. Rodney, D. & Proville, L. Stress-dependent Peierls potential: Influence on kink-pair activation. *Phys. Rev. B* **79,** 094108 (2009).
15. Gröger, R. & Vitek, V. Explanation of the discrepancy between the measured and atomistically calculated yield stress in body-centered cubic metals. *Phil. Mag. Lett.* **87,** 113–120 (2007).
16. Bulatov, V. V. & Cai, W. Nodal effects in dislocation mobility. *Phys. Rev. Lett.* **89,** 115501 (2002).
17. Caillard, D. Kinetics of dislocations in pure Fe. Part II. In situ straining experiments at low temperature. *Acta Mater.* **58,** 3504–3515 (2010).
18. Gilman, J. J. Escape of dislocations from bound states by tunneling. *J. Appl. Phys.* **39,** 6086–6090 (1968).
19. Indenbom, V. L., Petukhov, B. V. & Lothe, J. in *Elastic Strain Fields and Dislocation Mobility* (eds Indenbom, V. L. & Lothe, J.) 489–516 (Elsevier, 1992).
20. Gordon, P. A., Neeraj, T. & Mendelev, M. I. Screw dislocation mobility in BCC Metals: A refined potential description for α-Fe. *Phil. Mag. Lett.* **91,** 3931–3945 (2011).

21. Ventelon, L. & Willaime, F. Core structure and Peierls potential of screw dislocations in α-Fe from first principles: Cluster versus dipole approaches. *J. Computer-aided Mater. Des.* **14,** 85–94 (2007).
22. Henkelman, G., Uberuaga, B. P. & Jónsson, H. A climbing image nudged elastic band method for finding saddle points and minimum energy paths. *J. Chem. Phys.* **113,** 9901–9904 (2000).
23. Vineyard, G. H. Frequency factors and isotope effects in solid state rate processes. *J. Phys. Chem. Solids* **3,** 121–127 (1957).
24. Benderskii, V. A., Makarov, D. E. & Wight, C. A. *Chemical Dynamics at Low Temperature* (Wiley, 1994).
25. Johnson, D. F. & Carter, E. A. Hydrogen in tungsten: Absorption, diffusion, vacancy trapping, and decohesion. *J. Mater. Res.* **25,** 315–327 (2010).
26. Mrovec, M., Nguyen-Manh, D., Elsässer, C. & Gumbsch, P. Magnetic bond-order potential for iron. *Phys. Rev. Lett.* **106,** 246402 (2011).
27. Pizzagalli, L. & Beauchamp, P. First principles determination of the Peierls stress of the shuffle screw dislocation in silicon. *Phil. Mag. Lett.* **84,** 729–736 (2004).
28. Curtin, W. A., Olmsted, D. L. & Hector, L. G. A predictive mechanism for dynamic strain ageing in aluminum–magnesium alloys. *Nature Mater.* **5,** 875–880 (2006).
29. Ryu, S., Kang, K. & Cai, W. Entropic effect on the rate of dislocation nucleation. *Proc. Natl Acad. Sci. USA* **108,** 5174–5178 (2011).
30. Derlet, P. M., Nguyen-Manh, D. & Dudarev, S. L. Multiscale modeling of crowdion and vacancy defects in body-centered cubic transition metals. *Phys. Rev. B* **76,** 054107 (2007).
31. Ercolessi, F. & Adams, J. Interatomic potentials from first-principles calculations: The force-matching method. *Europhys. Lett.* **26,** 583–588 (1994).

Acknowledgements

This work was performed using HPC resources from GENCI-[CCRT/CINES] (Grant 2012096973). D.R. was supported by the Institut Universitaire de France.

Author contributions

All authors contributed equally to the present work.

Additional information

Supplementary information is available in the online version of the paper. Reprints and permissions information is available online at www.nature.com/reprints. Correspondence and requests for materials should be addressed to D.R.

Competing financial interests

The authors declare no competing financial interests.